RESEARCH ARTICLE

Anaerobic oxidation of methane in hypersaline cold seep sediments

Loïs Maignien[1], R. John Parkes[2], Barry Cragg[2], Helge Niemann[3,4], Katrin Knittel[3], Stephanie Coulon[1], Andrey Akhmetzhanov[5,6] & Nico Boon[1]

[1]Laboratory of Microbial Ecology and Technology (LabMET), Ghent University, Ghent, Belgium; [2]Laboratory of Geomicrobiology, Cardiff University, Cardiff, UK; [3]Max Planck Institute for Marine Microbiology, Bremen, Germany; [4] Department of Environmental Sciences, University of Basel, Basel, Switzerland; [5]National Oceanography Centre, Southampton, UK; and [6]LUKOIL Overseas UK Limited, London, UK

Correspondence: Loïs Maignien, Marine Biological Laboratory, 7 MBL street, 02543 Woods Hole MA, USA.
Tel.: +1 508 289 7282;
fax: +1 508 457 4727;
e-mail: lmaignien@mbl.edu

Received 20 April 2012; revised 28 July 2012; accepted 1 August 2012.
Final version published online 17 October 2012.

DOI: 10.1111/j.1574-6941.2012.01466.x

Editor: Julian Marchesi

Keywords
methane cold seep; Mercator mud volcano; sulphate reduction; 16S rDNA gene libraries; Gulf of Cadiz; Captain Arutyunov mud volcano.

Abstract

Life in hypersaline environments is typically limited by bioenergetic constraints. Microbial activity at the thermodynamic edge, such as the anaerobic oxidation of methane (AOM) coupled to sulphate reduction (SR), is thus unlikely to thrive in these environments. In this study, carbon and sulphur cycling was investigated in the extremely hypersaline cold seep sediments of Mercator mud volcano. AOM activity was partially inhibited but still present at salinity levels of 292 g L^{-1} (*c.* eightfold sea water concentration) with rates of 2.3 nmol cm^{-3} day^{-1} and was even detectable under saturated conditions. Methane and evaporite-derived sulphate comigrated in the ascending geofluids, which, in combination with a partial activity inhibition, resulted in AOM activity being spread over unusually wide depth intervals. Up to 79% of total cells in the AOM zone were identified by fluorescence *in situ* hybridization (FISH) as anaerobic methanotrophs of the ANME-1. Most ANME-1 cells formed monospecific chains without any attached partner. At all sites, AOM activity co-occurred with SR activity and sometimes significantly exceeded it. Possible causes of these unexpected results are discussed. This study demonstrates that in spite of a very low energy yield of AOM, microorganisms carrying this reaction can thrive in salinity up to halite saturation.

Introduction

Marine mud volcanoes (MV) are formed by the extrusion of fluidized sediments of deep origin to the sea floor (Milkov, 2000; Dimitrov, 2002; Kopf, 2002; Niemann & Boetius, 2010). Erupted material (mud breccia) often contains high amounts of methane and occasionally higher hydrocarbons (Kopf, 2002 and reference therein). The migration of hydrocarbons towards the sediment surface typically fuels a great variety of microorganisms and symbiotic fauna that harvest energy from these reduced molecules, directly or indirectly, using sea water electron acceptors (e.g. O_2, NO_3^-, SO_4^{2-}). Hydrocarbon seepage therefore promotes the development of thriving cold seep ecosystems, which support high standing stocks of free-living and symbiotic chemosynthetic microorganisms. One of the most important processes at cold seeps is the anaerobic oxidation of methane (AOM) coupled to sulphate reduction (SR; Knittel & Boetius, 2009 and references therein):

$$CH_4 + SO_4^{2-} \rightarrow HS^- + HCO_3^- + H_2O$$
$$\Delta G^{0\prime} = -16\,\text{kJ mol}^{-1}$$

On a global scale, this reaction oxidizes more than 80% of uprising CH_4 in the sea floor (Reeburgh, 2007 and references therein).

AOM is performed by three groups of *Euryarchaeota* related to methanogens: ANME-1, ANME-2 and ANME-3 (Hinrichs *et al.*, 1999; Boetius *et al.*, 2000; Orphan *et al.*, 2001, 2002; Knittel *et al.*, 2005; Niemann *et al.*, 2006b). These anaerobic methanotrophs often form consortia with sulphate-reducing bacteria (SRB) of the genera *Desulfosarcina/Desulfococcus* (DSS) or *Desulfobulbus* (Knittel

et al., 2003; Losekann *et al.*, 2007). On the basis of these observations, a syntrophic relationship between these microorganisms has been postulated (Boetius *et al.*, 2000; Orphan *et al.*, 2001) with an up to now unidentified interspecies transfer agent mediating electron transfer from methane-oxidizing ANME cells to their sulphate-reducing partners.

The typical geochemical signature of AOM activity in marine sediments is the presence of a so-called sulphate–methane transition zone (SMTZ), that is, opposed gradients of downward diffusing sulphate and upward migrating methane (Reeburgh, 2007 and references therein). Microorganisms mediating AOM are usually present and active in a narrow depth interval at the interface between these gradients (Knittel & Boetius, 2009 and references therein).

In addition to this sulphate-dependent mode, AOM may also be coupled to the reduction of oxidized metal species, such as Fe(III) and Mn(IV) (Beal *et al.*, 2009), and N species (Raghoebarsing *et al.*, 2006; Hu *et al.*, 2009; Ettwig *et al.*, 2010). So far, evidence for an environmental significance of these pathways, particularly in marine environments, is missing.

On the basis of an inventory of known metabolisms able to thrive in hypersaline environments, it has been proposed that the upper limit of salt concentration at which energy conservation can occur 'primarily depends on bioenergetic constraints' and secondly on the 'mode of osmotic adaptation used' (Oren, 1999, 2011). Balancing cell osmotic pressure by active ion pumping or the production of compatible solutes is indeed energetically costly and apparently excludes dissimilatory pathways characterized by low energy yields. From an energetic standpoint, it is thus surprising that a few studies could detect AOM in hypersaline environments (Oren, 2011 and references therein). Yet, the influence of salinity on AOM activity and microbial community composition is not well constrained. One study, for instance, found geochemical and molecular evidence for AOM activity mediated by ANME-1/SRB in hypersaline sediment of the Gulf of Mexico (Lloyd *et al.*, 2006), while a recent study on a deep-sea brine pool and a MV, in contrast, suggested that presence of hydrogen prevented AOM activity in spite of the presence of both methane and sulphate (Joye *et al.*, 2009). Circumstantial evidence indicates a dominance of ANME-1 over the other ANME groups in hypersaline settings, thus suggesting that this clade might be more tolerant to high salinity (Daffonchio *et al.*, 2006; Lloyd *et al.*, 2006; Yakimov *et al.*, 2007; Niederberger *et al.*, 2010; La Cono *et al.*, 2011). Nevertheless, significant ANME-1 populations are also found in nonhypersaline methane seeps, for example, in the Eel River Basin (off California), the Black Sea microbial mats, the Hydrate Ridge (off Oregon) or the North Sea Tommeliten seeps (Supporting information, Data S1; Orphan *et al.*, 2002; Knittel *et al.*, 2005; Niemann *et al.*, 2005; Treude *et al.*, 2005).

Recently, a hypersaline mud volcano (Mercator MV) that bears large amounts of methane was discovered in the Gulf of Cadiz, East Atlantic (Van Rensbergen *et al.*, 2005; Nuzzo *et al.*, 2009; Scholz *et al.*, 2009; Perez-Garcia *et al.*, 2011). This provides a very good opportunity to study the microbial ecology of methane and sulphur cycling in a deep-sea hypersaline environment. Here, we document for the first time the microbial activity and community structure in relation to geochemical settings at Mercator MV, with the aim to understand the functioning of AOM communities under extreme hypersaline conditions. Our results are compared with those from Captain Arutyunov MV (CAMV), a nonhypersaline MV in the vicinity of the Mercator MV.

Materials and methods

Coring and sampling

Gravity or piston corer, and mega corer (GC, PC and MC, respectively) were deployed at each of the Mercator MV sites. Sediment recovery largely varied between cores, probably due to the presence of large halite/gypsum crystals, hard grounds in shallow subsurface or dry sediment horizons. Cores with enough sediment recovery for downstream analysis were selected for this study. Upon recovery, GCs and PCs were cut into 1-m sections and stored at 4 °C until further processing (< 10 h after recovery). MCs as well as GC and PC core sections were subsampled by extruding sediments from the core using a plunger.

Geochemistry

Pore water was extracted from 25 mL sediment using a pore water press (Reeburgh, 1967) equipped with 0.45-μm pore-size nitrocellulose filters. Pore water was then filtered through 0.1-μm pore-size filters prior to sample storage. For sulphide measurement, 1 mL of pore water was preserved in 500 μL zinc acetate solution (10% w/v). AVS was extracted from sediment sealed in a glass jar by adding 6 N HCl under continuous N_2 flow collected in a 7 mL Zn acetate trap, using the experimental setup described in the study by Kallmeyer *et al.* (2004). Concentration of both dissolved and AVS was measured colorimetrically using the methylene blue method (Cline, 1969). Sulphate, chloride and acetate were measured by ion chromatography as described in the study by Parkes *et al.* (2007). Methylated amines were analysed using a DX-120 (DIONEX, Camberley, UK) fitted with an IonPac CS16 column coupled with a CSRS 300 4 mm suppressor

and a conductivity detector. Separation of pore water constituents was achieved using methanesulphonic acid eluent (25 mM) at a flow rate of 0.75 mL min^{-1}. Prior to analysis, samples were diluted 1 : 15 (v/v) in ultrapure deionized water (Milli-Q) for samples with sea water levels of chloride and 1 : 159 (v/v) for sample with higher chloride concentrations. Maximum concentration observed in pore water samples from both MV was far below the accurate detection limit of the method (*c.* 400 μM as determined empirically). The highest methylamine concentration was about 5 μM, indicating the most probable detection limit of the method. This value was taken as an upper limit for pore water methylamine pool and used to calculate maximum potential methylamine MG (see *ex situ* rate measurement below).

Dissolved gas in pore water was analysed on shore according to the study by Parkes *et al.* (2007): 2 cm^3 of sediment (sampled with a 5 mL cut-off syringe) was transferred into a glass vial containing 6 mL NaOH (2.5%, w/v), which was then immediately sealed with a butyl rubber septum and stored upside down. The headspace was analysed for H_2, CH_4 and higher volatile hydrocarbons with a modified two channels Perkin Elmer/Arnel 2101 natural gas analyser. Channel A was equipped with three columns (1/8″SF*2.5′ 30% DC-200 on Chromosorb PAW80/100, 1/8″SF*30′ 30%DC-200 on Chromosorb PAW 80/100 and 1/8″SF*6′ ASAG 60/80, respectively) and with both a thermal conductivity and a flame ionization detector (TCD and FID). FID was operated at 45 mL min^{-1} hydrogen and 450 mL min^{-1} air. Channel B was also equipped with three columns (1/8″SF*6′Silica Gel 60/80, 1/8″SF*4′HayeSep T 60/80 and 1/8″SF*9′Molecular Sieve 5A 45/60) and a TCD. The system was run under isothermal conditions (110 °C). Compound assignment and quantification were carried out by direct comparison with known standards (Scott Specialty Gases). Dissolved inorganic carbon concentrations ($\sum CO_2$) were determined from 1.25-mL samples of pore water, fixed with 20 mL HgCl2 and sealed, without headspace, in a glass vial using the rapid small volume flow injection method of measuring aqueous CO_2 (Hall & Aller, 1992) with the gas analyser described above.

Ex situ rate measurements

For AOM and SR rates measurements, cores were subsampled with mini cores (polycarbonate tube, diameter 2.5 cm, length 20 cm) with silicone-sealed side injection ports spaced every 2 cm, or with glass barrels (diameter 1 cm, length 6 cm) with a syringe plunger at one end, and a butyl rubber stopper at the other end as injection port (for details see Treude *et al.*, 2005). Within 2 h after sampling, methane radiotracer (25 μL of aqueous $^{14}CH_4$ solution, 5 KBq) or sulphate radiotracer (5 μL of aqueous $^{35}SO_4^{2-}$ solution, 60 KBq) was injected through the injection ports, and samples were incubated for 24 h in the dark at *in situ* bottom water temperature measured during ROV dives (e.g. 13 °C for Mercator MV stations and 4 °C for CAMV). After incubation, AOM and SR reactions were stopped by transferring the samples into glass flasks containing 25 mL NaOH (2.5% w/v) or 50-mL plastic tubes containing 20 mL zinc acetate solution (20% w/v), respectively. Methane and sulphate turnover was determined as described elsewhere (Jørgensen, 1978; Treude *et al.*, 2003; Kallmeyer *et al.*, 2004). AOM and SR rates were determined as the product of turnover and methane or sulphate concentration, respectively. For AOM rates, methane concentration was corrected for maximum solubility at ambient pressure during incubations (i.e. 1 bar) and *in situ* salinity (Duan & Mao, 2006).

Rates of MG were measured as described in the study by Parkes *et al.* (2007). Briefly, sediment was subsampled using either mini cores (diameter 1.5 cm, length 10 cm) with silicone-filled side injection holes (4 μL substrate per 1 cm depth interval) or 10-mL cut-off syringes closed with rubber stoppers (7.5 μL substrate per syringe). The samples were preincubated for 24 h in nitrogen-flushed gas-tight bags to allow methane concentration equilibration prior to radiotracer injection. ^{14}C-labelled carbonate (10 KBq μL^{-1}), acetate (6 KBq μL^{-1}), methanol (2.05 KBq μL^{-1}) or methylamine (7.25 KBq μL^{-1}) were injected, and samples were incubated at *in situ* bottom water temperature for 7–21 h in nitrogen-flushed gas-tight bags. Microbial reactions were then stopped by transferring incubations into glass jars containing 7 mL of 1 M NaOH. In the laboratory, ^{14}C methane was determined as for AOM. Substrate turnover was determined according to the radioactivity of the trapped CO_2 and the amount of added label in the product pool. Rates were calculated as the product of turnover values times total CO_2 or acetate concentrations. For methylamine MG, rates were obtained by multiplying the substrate turnover value by an arbitrary methylamine concentration of 5 μM (as methylamine concentration in pore water was consistently below detection limit). Me-MG rates should thus be considered as maximum potential rates rather than actual *ex situ* rates.

Nucleic acid extraction and amplification

At Mercator Rim 1 (32–33 cmbsf depth interval), environmental DNA was extracted from five replicates sediment sample, each of 0.3 g sediment, using the PowerSoil DNA extraction Kit (MoBio Labconsult, Brussels, Belgium) according to manufacturer recommendations. 16S rRNA genes were amplified using Arch20f/Uni1392r primer pair for Archaea (Kane *et al.*, 1993; Massana *et al.*,

1997) and GM3f/GM4r primer pair for Bacteria (Muyzer *et al.*, 1995). PCR conditions were as in the study by Losekann *et al.* (2007). PCR were carried out in triplicate, amplicons were pooled and purified (PCR purification kit, Qiagen).

Clone libraries construction, screening and phylogeny inference

Purified PCR products were ligated in the PCR-2.1 vector and cloned into Top10 chemocompetent cells using TOPO-TA cloning kit (Invitrogen, Merelbeke, Belgium). The size of the insert was verified with a colony PCR on overnight grown positive transformants using M13 vector-specific primer pair (Invitrogen). M13 PCR amplicons were used for ARDRA of the libraries with AluI and RsaI (Fermentas, St. Leon-Rot, Germany). Digested DNA was run on a 3% agarose gel, and images were analysed with the BIONUMERICS software (Bionumerics, Kortrijk, Belgium). Clones were clustered according to restriction pattern using the Jaccard similarity index, and when a cluster contained multiple clones, at least two representative clones were sequenced. Bidirectional sequencing was carried on ABI-3730xl sequencer (Applied Biosystem, Lennik, Belgium) at the Genetic Service Unit of the Ghent University Hospital using M13 vector primers.

Sequence accession numbers

Sequences from this study are published in GenBank under the accession numbers FJ813536, FJ813545–FJ813556, FJ813561–FJ813564, FJ813569, FJ813573, FJ813576, FJ813591, FN820294, FN820296, FN820299, FN820302, FN820303, FN820307, FN820308, FN820310, FN820311, FN820312, FN820317, FN820319, FN820320–FN820327, FN820331–FN820335, FN820338, FN820355, FN820359, FN820367, FN820370, FN820372, FN820375, FN820376, FN820377, FN820381, FN820382, FN820384, FN820385, FN820386, FN820390, FN820402–FN820411, FJ813544.

Phylogenetic tree reconstruction and phylotype inference

All sequences were aligned with the online SINA webaligner of SILVA (Pruesse *et al.*, 2007); http://www.arb-silva.de) and imported together with nearly full length (> 1200 bp for bacterial sequences and > 900 bp for archaeal sequences) closely related 16S rRNA gene sequences in the ARB SILVA database release 102. Sequences were further clustered by OTU (98% similarity cutoff) with the MOTHUR software (Schloss *et al.*, 2009). Phylogenetic trees were reconstructed using the maximum likelihood-based PhyML algorithm (http://www.atgc-montpellier.fr/phyml/; Guindon *et al.*, 2009), filtering out most variable positions of the alignment (50% cut-off). Bootstrap values associated with tree nodes were calculated using the aLRT method (Anisimova & Gascuel, 2006).

Fluorescence *in situ* hybridization (FISH) and catalysed reporter deposition fluorescence *in situ* hybridization (CARD-FISH) cell staining and microscopic observations

On board, 2 cm^3 of sediment was fixed by resuspending with 3 mL of filter-sterilized (0.2 μm) formaldehyde in sea water solution (3% v/v final concentration) for 4 h at 4 °C. Samples were then washed three times with 10 mM phosphate-buffered saline (pH 7.5, 150 mM NaCl) and resuspended in 1 : 1 v/v PBS/ethanol solution and stored at -20 °C. FISH and CARD-FISH procedures were carried out according to the study by Pernthaler *et al.* (2001, 2002). For CARD-FISH, the following modifications were applied: for permeabilization of rigid archaeal cell walls, 15 μg mL^{-1} proteinase K was used (3 min at room temperature); for bacterial cell wall permeabilization, 10 mg mL^{-1} lysozyme (15 min at 37 °C). Horseradish-peroxidase- (CARD-FISH) or Cy3-labelled (FISH) probes targeting the following groups were used: probes Eub338 I-III (Daims *et al.*, 1999) specific for most bacteria (35% formamide in hybridization buffer or FA), probe Arch915 (Stahl & Amann, 1991) specific for most Archaea (35% FA), probe ANME1-350 (Boetius *et al.*, 2000) specific for ANME-1 (40% FA), probe EelMS-932 (Boetius *et al.*, 2000) specific for ANME-2 (40% FA), probe ANME-3-1249 with unlabelled helper oligonucleotides ANME3-1243 and 1249 h (Losekann *et al.*, 2007) specific for ANME-3 (40% FA) and probe DSS658 (Manz *et al.*, 1998) specific for the *Desulfosarcina/Desulfococcus* branch of *Deltaproteobacteria* (60% FA), including Seep-SRB subgroups. Cells were counterstained with 1 μg mL^{-1} 4′,6-diamidino-2-phenylindole (DAPI) for 10 min. Hybridized cells were examined under an epifluorescence microscope (Carl Zeiss Axioplan, Jena, Germany). For each sample and probe, 50 independent microscopic fields of view were counted, corresponding to approximately 400-800 DAPI-stained cells, and the fraction of double-stained cells has been determined.

Results

Site description and sampling

The Mercator MV was located at 350 m water depth in the Gulf of Cadiz, at *c.* 50 km off Morocco (Fig. 1a). Concentric rims visible on the high-resolution bathymetric map were interpreted as successive eruptive events

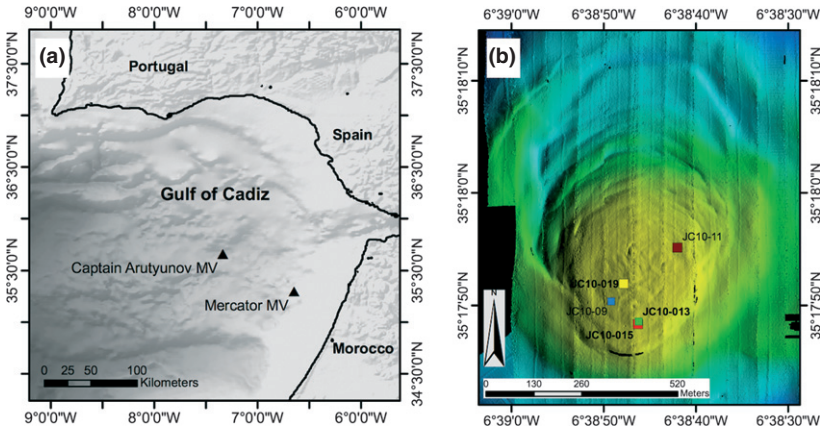

Fig. 1. Study location and sampling stations. (a) Gulf of Cadiz bathymetric map showing the location of the two MV investigated in this study. (b) High-resolution bathymetric maps of the Mercator mud volcano, located in the shallow region of the Gulf of Cadiz. This MV was cored in the Crater Centre (JC10-09 and -19), northern Rim (JC10-11) and southern Rim (JC10-13 and -15).

Table 1. Sampling stations. Names, coring device used, coordinates, water depth and size of the recovered sediment column at each site of this study. Note that Rim 1 and Rim 2 sites are replicate cores of the same location with different coring devices

Location	Station	Core name	Core type	Latitude	Longitude	Depth (m)	Length (cm)
Reference		JC10-02	Mega core	35°17.260N	6°40.240W	470	42
		JC10-04	Piston core	35°17.244N	6°40.251W	470	375
Mercator MV	Crater Center	JC10-09	Gravity core	35°17.840N	6°38.820W	349	80
		JC10-019	Piston core	35°17.866N	6°38.797W	346	272
	Rim 1	JC10-013	Mega core	35°17.810N	6°38.770W	348	28
	Rim 2	JC10-015	Gravity core	35°17.806N	6°38.771W	346	93
	Rim 3	JC10-11	Mega core	35°17.920N	6°38.700W	351	40
CAMV	Crater Center	JC10-066	Piston core	35°39.637N	7°20.046W	1311	408

and permitted to estimate the position of the physical crater centre where the most recently expelled mud and highest fluid flux were expected, as well as at three rim sites (Fig. 1 and Table 1). At Mercator MV Crater Centre site, gas was venting from the seafloor, and large halite (NaCl) and gypsum ($CaSO_4$) crystals were recovered from the sediments between 150 and 200 cm below the sea floor (cmbsf). CAMV was sampled in the crater centre site. For comparison with non-MV sediments, a reference station was sampled 2.4 km NE of Mercator MV. Details of the high-resolution bathymetry method, sampling sites description and coring devices are given in Data S1.

Geochemistry

As Na^+ and Cl^- are the major brine-derived ions present in the pore water of Mercator MV (Scholz *et al.*, 2009) and CAMV (Hensen *et al.*, 2007); the salinity in these sediments was estimated by the chloride concentration (Fig. 2). At the Mercator MV Crater Centre (cores JC10-09 and -19), chloride concentration at 10 cmbsf was already 3.5-fold (2011 mM) higher than sea water values

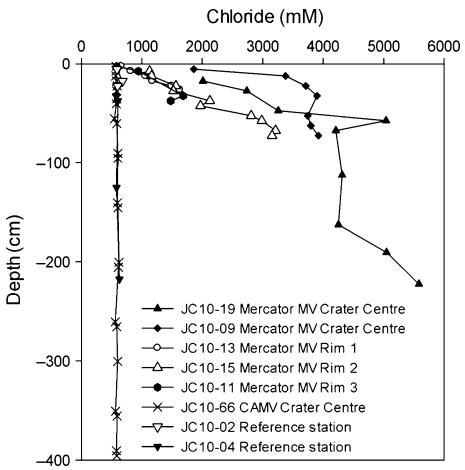

Fig. 2. Sediment salinity. Comparison of chloride concentration profiles used to estimate salinity in the sediments of Mercator MV and CAMV.

and further increased with depth along concave up gradients, up to halite saturation level (*c.* 5800 mM) at 220 cmbsf. At the rim stations (cores JC10-11, -13 and -15),

chloride concentration formed a quasi-linear gradient with depth from sea water concentration (*c.* 580 mM) at the surface up to 3213 mM at 67.5 cmbsf. Both at the reference station (cores JC10-02 and -04) and at CAMV Crater Centre stations (core JC10-66), chloride concentration reflected sea water concentration at the sediment surface and remained constant with depth. On the basis of these different salinity profiles, three methane-rich habitats with decreasing salt contents (chlorinity gradients) were selected for further detailed studies on geochemistry and microbial activity: (1) hypersaline sediments (core JC10-19) hereafter named Mercator MV Crater Centre, (2) sediments with lower but still elevated salinity (cores JC10-13 and JC10-15) hereafter named Mercator MV Rim 1 and Rim 2, respectively and (3) sediments with regular sea water salinity (core JC10-66) hereafter named CAMV Crater Centre.

Methane

At all three locations, an upward migration of methane in the sediment was indicated by elevated methane concentrations in deeper section of the cores, generally decreasing towards surface (Fig. 3). These results are in agreement with previous publications on the geochemistry of the chosen structures (e.g. Van Rooij *et al.*, 2005; Niemann *et al.*, 2006a; Hensen *et al.*, 2007; Nuzzo *et al.*, 2009; Scholz *et al.*, 2009). At Mercator MV Crater Centre, methane concentration decreased from 3 mM at 75 cmbsf to 0.6 mM at the sediment surface. At Mercator MV Rim 1, the methane decreased from 0.23 mM at 21 cmbsf to 5.10^{-3} mM at 11.5 cmbsf, and similar trend was observed at Mercator MV Rim 2. At CAMV Crater Centre, methane concentration steeply decreased from 1.2 mM at 26.5 cmbsf to near background concentrations at 21.5 cmbsf, and methane was depleted in the upper 20 cm of the core.

Sulphate

Sulphate concentration was close to sea water values at the sediment surface (28–30 mM) in all cores (Fig. 3). At Mercator MV, sulphate first decreased with depth down to 13.2 mM at Crater Centre or to 24.4 mM at Rim 2 (at 162 and 42 cmbsf respectively), but then increased again with depth, reaching maximum values of 18.5 and 28.3 mM, respectively. At Mercator MV Rim 1, sulphate concentration remained constant down to 28 cmbsf. At CAMV Crater Centre, sulphate concentration steeply decreased and reached 2.8 mM at 22.5 cmbsf, remained at this level down to 40.5 cmbsf and was below detection limit (*c.* 0.1 mM), below 55 cmbsf.

Sulphide

At all Mercator MV sites, we could not detect any soluble sulphide (H_2S, HS^-, S_2^-; data not shown), although decreasing sulphate contents and sulphate reduction rates (SSR; see next section) indicated sulphide production. However, at least some of the sulphide could be precipitated because acid volatile sulphide (AVS) content was elevated (0.5 mM of sediment) at Mercator MV Rim 2 (32 cmbsf; data not shown). In contrast, at CAMV Crater Centre, we could detect substantial amounts of (dissolved) sulphide peaking with 3.2 mM at 22.5 cmbsf (Fig. 3d), that is, at the interface between the methane and sulphate gradients.

Acetate and hydrogen

Acetate was present in the pore water of all sites (Fig. 3) with decreasing concentrations from the deeper layers (between *c.* 40 μM at Mercator Rim sites to *c.* 90 μM at Mercator Crater Centre) towards the surface (5–20 μM). At CAMV Crater Centre, a peak of acetate (107 μM) occurred at 40 cmbsf. Substantial amounts of dissolved hydrogen, mostly as discrete concentration peaks, could be detected in all four cores (Fig. 3). Maximum hydrogen concentration ranged from 0.7 nM at Mercator Crater Rim 2 to 4.4 nM at Mercator Crater Centre. These values probably represent low estimates owing to sediment degassing during recovery.

Microbial activity

Anaerobic oxidation of methane

Significant rates of AOM (AOMR) were detected in all habitats investigated in this study (Fig. 3). At Mercator MV Crater Centre (Fig. 3a), AOM activity was present throughout the entire core, with two zones of apparently higher activity: in the first 50 cm below the surface, with a maximum AOMR of 6 nmol cm^{-3} day^{-1} at 21 cmbsf, and at greater depth (170 cmbsf) with a maximum AOMR of 2.3 nmol cm^{-3} day^{-1}. Notably, both maxima coincided with a decrease in methane concentrations (Fig. 3). At Mercator MV Rim 1 and Rim 2 (Fig. 3b and c), AOM activity was present in near-surface sediments with rates of 0.8 and 2 nmol cm^{-3} day^{-1}, respectively, and decreased with depth to values close or below detection limit. At 25 cmbsf, AOMR increased, and two activity peaks of 3.0 and 3.6 nmol cm^{-3} day^{-1} were detected between 30 and 40 cmbsf at Rim 1, and a single peak of 8.5 nmol cm^{-3} day^{-1} at Rim 2. At the latter, AOM activity extended down to the bottom of the core, with rates between 1 and 1.7 nmol cm^{-3} day^{-1}. At CAMV Crater

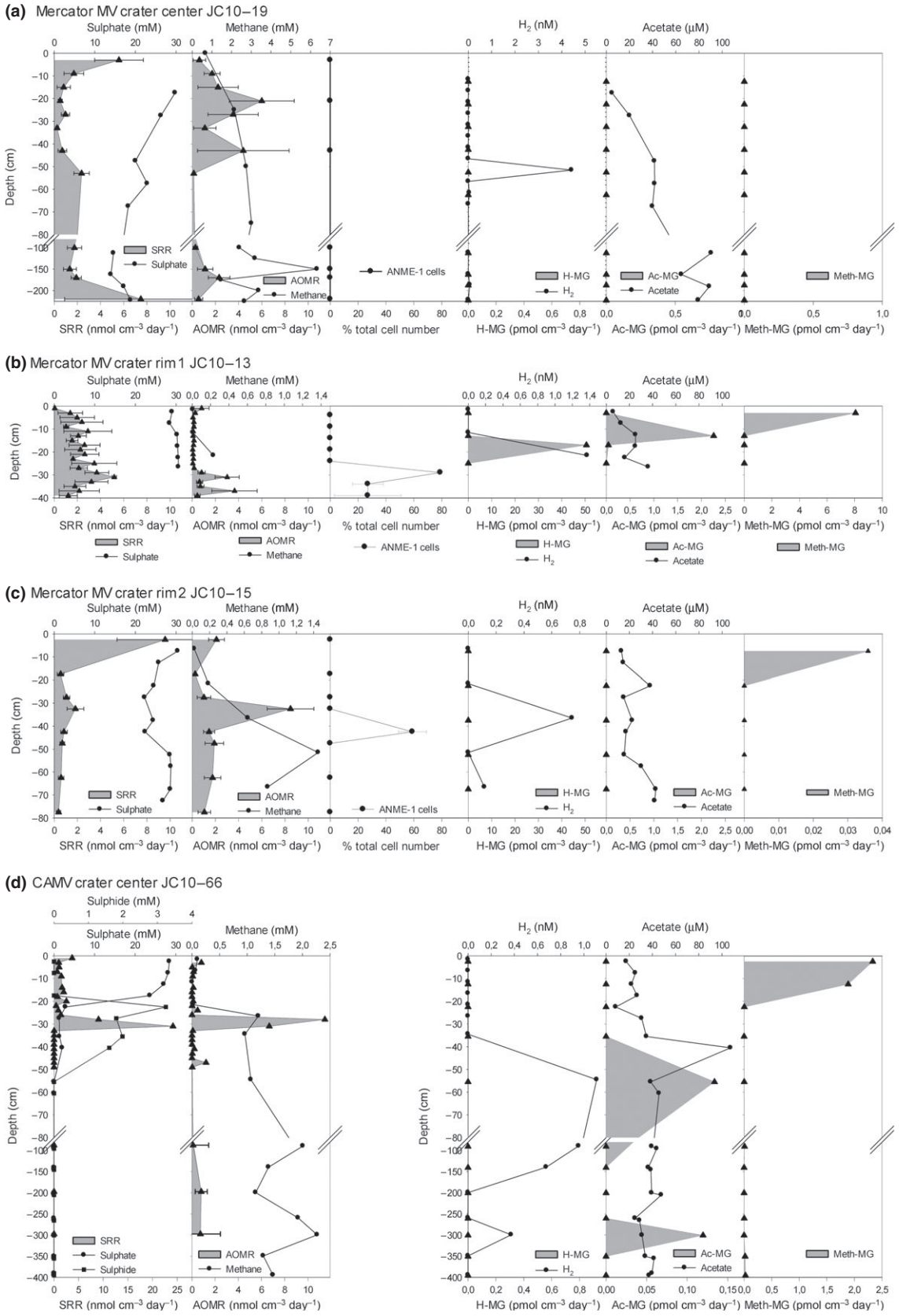

Fig. 3. Geochemistry and microbial activity at Mercator MV and CAMV. AOM, SR and MG activities at each station (triangle) were plotted with their respective substrate/product concentration profiles (methane, sulphate/sulphide, hydrogen, acetate). Methanol MG turnover was below detection limit in all locations. Meth-MG thus only refers to methylamine MG rates. These are given based on a methylamine concentration of 5 μM in sediment pore water (see Experimental procedures). H-MG and Ac-MG refer to hydrogenotrophic and acetotrophic MG, respectively. Note the scale difference for methane at Mercator MV Crater Centre (a) and for SRR and methane at CAMV (d). Error bars correspond to ± one standard error of the mean (n = 3) when replicates were taken.

Centre (Fig. 3d), a distinct peak of AOM activity (11.4 nmol cm^{-3} day^{-1}) was found between 28 and 31 cmbsf, which vertically coincided with the sulphide peak and the depth of the sulphate–methane transition. AOM was close to the detection limit above this active zone. As already observed by Niemann *et al.* (2006a), weak AOMR (0.5–1.3 nmol cm^{-3} day^{-1}) were detected below the SMTZ between 47 and 297 cmbsf.

Sulphate reduction

At Mercator Crater Centre (Fig. 3a), SRR showed three maxima: immediately below the surface (SRR of 5.58 nmol cm^{-3} day^{-1} at 5 cmbsf), at 56 cm (2.36 nmol cm^{-3} day^{-1}) and at 220 cmbsf (7.47 nmol cm^{-3} day^{-1}). At Mercator MV Rim 1 (Fig. 3b), SR was scattered over depth, but showed a general increase towards 30 cmbsf, broadly corresponding to depth of the two AOM maxima. At Mercator MV Rim 2 (Fig. 3c), SR was maximal just beneath the sediment surface (9.6 nmol cm^{-3} day^{-1}) and showed a second lower maximum of 1.83 nmol cm^{-3} day^{-1} at the same depth (31 cmbsf) where also the AOM maximum was found. At CAMV Crater Centre, in contrast to the rather weak coupling between AOM–SR found at Mercator MV, SR peaked (24.13 nmol cm^{-3} day^{-1}) just in the same sediment horizon (28–31 cmbsf) where also AOM was maximal.

Depth integrated AOM rates (∑AOMR) and SR rates (∑SRR) were comprised between 147 and 898 mmol m^{-2} $year^{-1}$, and 326 and 1803 mmol m^{-2} $year^{-1}$, respectively (Table 2). Remarkably, AOMR exceeded SRR in several sediments intervals. This difference was significant (i.e. no overlap of 95% confidence intervals) at Mercator MV Rim 2 (37.5 cmbsf) and in most sediment horizons between 7 and 29 cmbsf at Mercator MV Crater Centre. As a consequence, ∑AOMR exceeded ∑SRR by a factor 2.8 at Rim 2 in the 27–77 cmbsf interval, 1.23 over the entire core (Table 2), and 2.2 at Crater Centre between 7 and 49 cmbsf.

Methanogenesis

With the exception of Mercator MV Crater Centre, methanogenesis (MG) using different substrates could be detected in all cores, albeit at very low rates and at discrete depth horizons. No methanol MG was observed in any of the sites investigated. Generally, we found a vertical succession of methylotrophic (Meth-MG) with methylamine as a substrate in the shallowest horizons, followed by acetotrophic (Ac) and then by hydrogenotrophic (H) MG. At Mercator MV Rim 1 (Fig. 3b), Meth-MG peaked with 8.1 pmol cm^{-3} day^{-1} at 3 cmbsf, Ac-MG with 2.3 pmol cm^{-3} day^{-1} at 13 cmbsf and H-MG with 50.5 pmol cm^{-3} day^{-1} at 17 cmbsf. At Rim 2 (Fig. 3c), a peak of Meth-MG was also present near sediment surface, but we could not detect H-MG or Ac-MG. Similarly, at CAMV Crater Centre, H-MG was absent, but we found two peaks of Ac-MG at 55 and 300 cmbsf (*c.* 0.13 pmol cm^{-3} day^{-1}) and a near-surface peak in Meth-MG (Fig. 3d).

Table 2. Areal microbial activity rates. Areal rates ∑SRR and ∑AOMR were obtained by integrating volumetric AOMR and SRR over the entire core (total) or the over the SMTZ. The AOM contribution to SR over the entire core (resp. over the SMTZ) is given by the ratios ∑AOMR (total)/∑SRR (total) [resp. ∑AOMR (total)/∑SRR (SMTZ)]. In the absence of an SMTZ in Mercator MV sediments, the latter ratio does not apply to these sites

Station	Core JC10-	Flux (mmol m^{-2} $year^{-1}$)			Depth integrated rates (mmol m^{-2} $year^{-1}$)				
		Sulphate	Sulphide	Methane	∑SRR Total	∑SRR SMTZ	∑AOMR Total	∑AOMR (total)/∑SRR (SMTZ)	∑AOMR (total)/∑SRR (total)
Mercator MV									
Crater Centre	19	n.d.	n.d.	43	1803	n.a.	898	n.a.	0.50
Rim 1	13	n.d.	n.d.	20	326	n.a.	80	n.a.	0.25
Rim 2	15	n.d.	n.d.	26	458	n.a.	562	n.a.	1.23
CAMV									
Crater Centre	66	1033	653	171	435	232	147	0.63	0.34

n.d., not determined; n.a., not applicable.

Microbial community structure

The structure of the microbial community involved in AOM in hypersaline sediments of Mercator MV Rim 1 was investigated by constructing both archaeal (85 clones) and bacterial (75 clones) 16S rRNA gene libraries with DNA extracted in the 32–33 cmbsf interval where AOM was maximum. Amplified ribosomal DNA restriction analysis (ARDRA) of these clones resulted in 17 archaeal and 47 bacterial groups displaying different restriction patterns for which at least two representative clones were sequenced. These sequences clustered into 4 and 22 operational taxonomic units (OTUs), respectively. Nonparametric Chao 1 richness estimators (8) were of 7 and 33, thus resulting in library richness coverage of 57% for the archaeal library and of 67% for the bacterial library. Rarefaction curves computed with the MOTHUR software (Schloss *et al.*, 2009) indicated that the Archaeal diversity was extensively covered by the library, whereas bacterial curve did not reach a plateau (see Data S1).

Sequences belonging to the ANME-1b clade (Hinrichs *et al.*, 1999) largely dominated the archaeal library (n = 69/85, Fig. 4), followed by sequences belonging to the GoM-Arc1 clade (n = 14/85; Lloyd *et al.*, 2006); also called ANME-2d by Mills *et al.* (2003, 2004). Most bacterial sequences were affiliated with SRB belonging to the *Deltaproteobacteria* (n = 50/75, Fig. 5). Of these, sequences belonging to the Seep-SRB1 cluster (Knittel *et al.*, 2005) constituted the largest fraction (n = 39/75) of the bacterial diversity, falling in the Seep-SRB1-c (n = 30/75), Seep-SRB1-d (n = 7/75) and Seep-SRB1-a (n = 2/75), the putative syntrophic ANME partners subgroups (Schreiber *et al.*, 2010). In addition, sequences falling within the families *Anaerolineacea* (n = 1/75) and

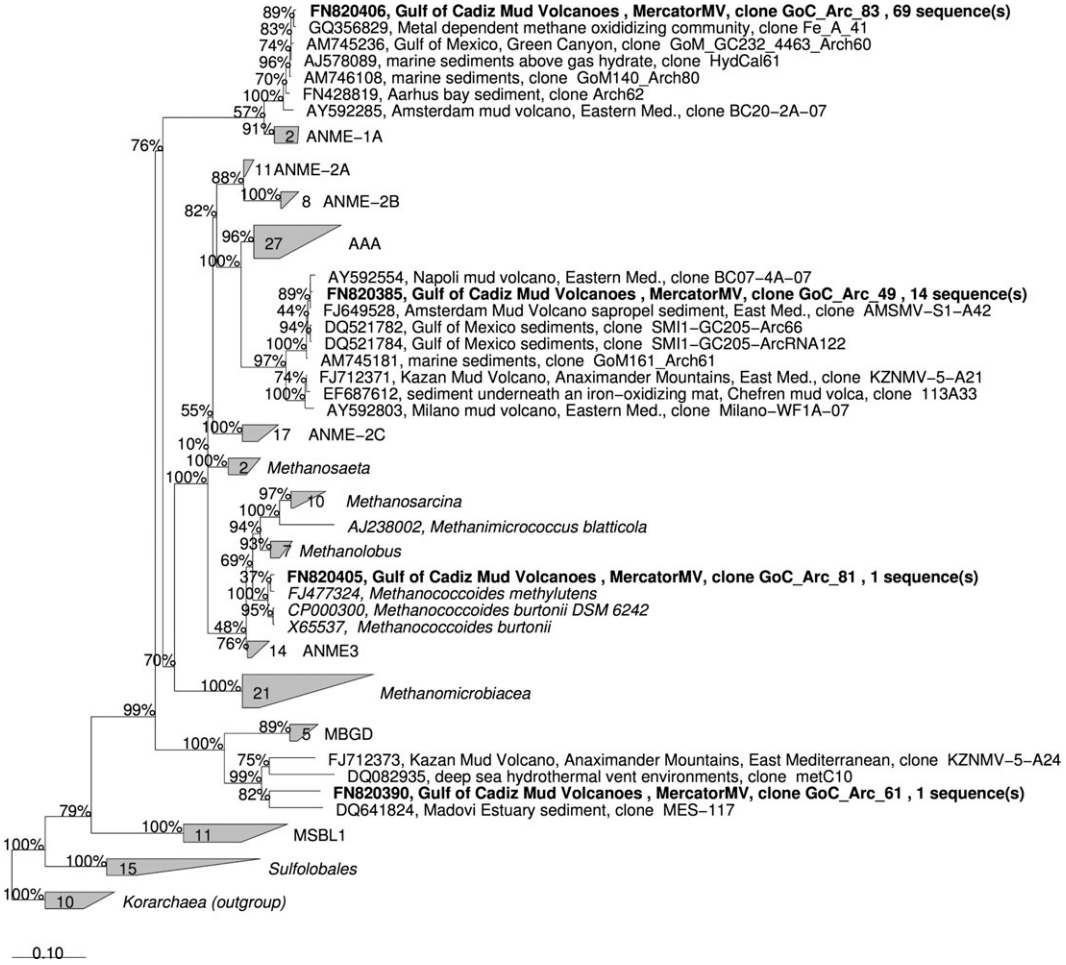

Fig. 4. Affiliation of Archaeal 16S rRNA gene sequences from Mercator MV Rim 1 (32–33 cmbsf). The phylogenetic tree was reconstructed based on a subset of 351 sequences using the maximum likelihood method (PhyML, Guindon *et al.*, 2009) filtering out positions according to base frequencies among Archaea (50% cutoff). Percentages indicate branch support as calculated by the aLRT bootstrapping method (Anisimova & Gascuel, 2006; Guindon *et al.*, 2009).

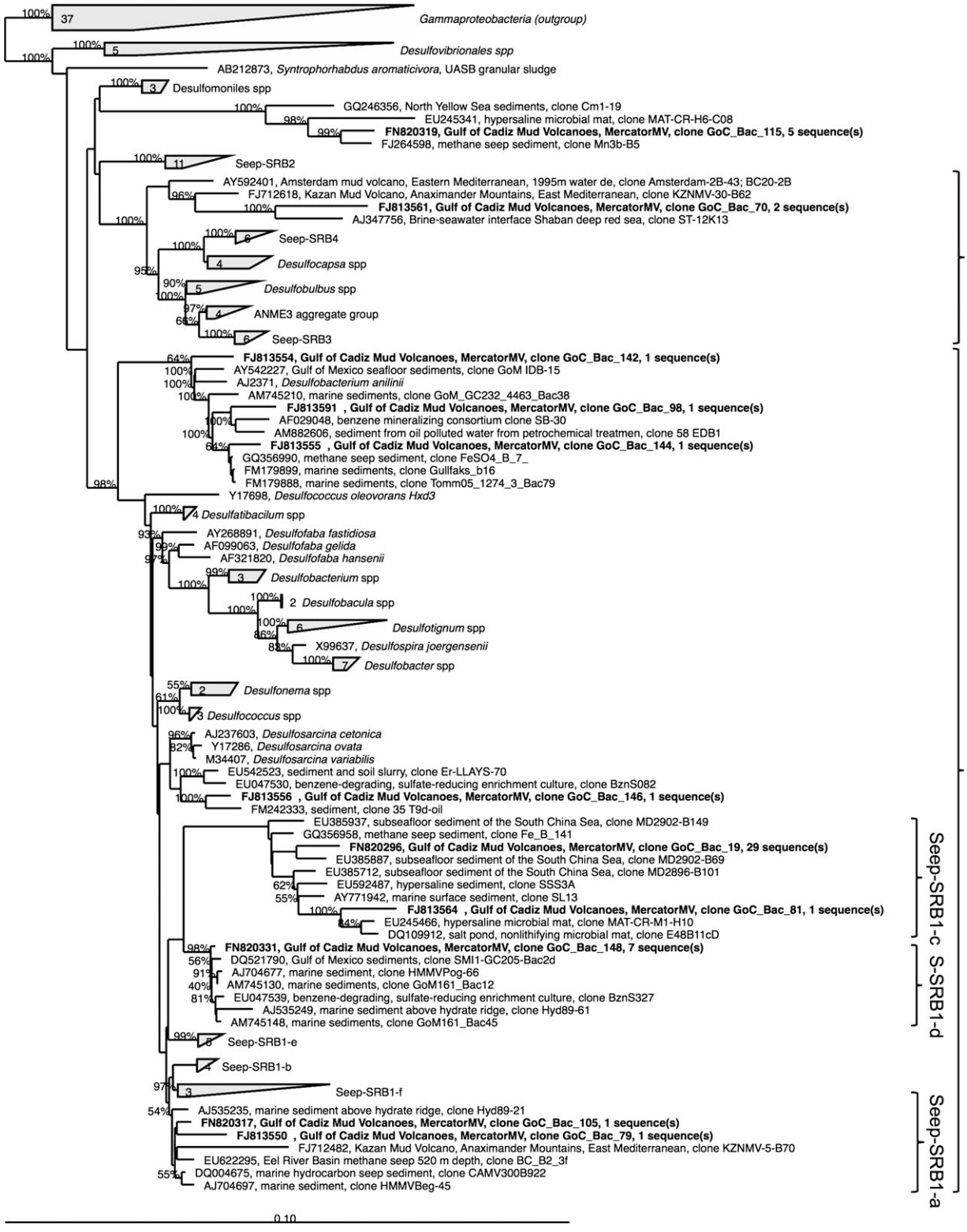

Fig. 5. Affiliation of bacterial 16S rRNA gene sequences from Mercator MV Rim 1 (32–33 cmbsf). The phylogenetic tree was reconstructed based on a subset of 195 sequences using the maximum likelihood method (PhyML, Guindon *et al.*, 2009) filtering out positions according to base frequencies among *Deltaproteobacteria* (50% cutoff). Percentages indicate branch support as calculated by the aLRT bootstrapping method (Anisimova & Gascuel, 2006; Guindon *et al.*, 2009).

Spirochetacea (n = 1/75) were present in the library. The remaining bacterial phylotypes were mostly affiliated with candidate phyla with no cultivated representatives, such as candidate divisions OP8 (n = 11/75), OP9 (n = 1/75), WS3 (n = 1/75) and TA06 (n = 6/75).

The *in situ* abundance and distribution of putative archaeal anaerobic methanotrophs (ANME-1, -2 and -3) were further investigated in the three Mercator MV cores applying CARD-FISH or FISH at CAMV Crater Centre. Confirming the results of the archaeal clone library, ANME-1 was the only group of known methanotrophs detected at Mercator MV. Members of this clade were found at several depth intervals. At Mercator MV Rim 1, ANME-1 cells were dominant at 29 cmbsf, accounting for 79 ± 0.8% of the DAPI-stained cells (Fig. 3c). At the same depth, 75% of the DAPI-stained cells belonged to the domain Archaea, indicating that most likely all of these were ANME-1 cells (results not shown). In general, ANME-1 cells were rod-shaped, formed chains of 2–16 cells (Fig. 6a and b) and were not associated with other type of cells. Less than 10% of ANME-1 cells were involved in large aggregates (Fig. 6c and d) comprising few non-ANME-1 coccoid cells. Bacteria accounted for 21% of DAPI-stained cells, of which 53% (i.e. 11% of the total cell number) belonged to the DSS group, which includes the Seep-SRB cluster of putative ANME partners. However, no direct cell–cell contact of DSS cells and ANME-1 was observed. At Mercator MV Rim 2, ANME-1 cells were only observed at 42.5 cmbsf and constituted 58 ± 10% of the DAPI-stained cells (Fig. 3c). There, cells were smaller (*c.* 0.7 μm), with coccoid or short rod shapes, and found as single cells or chains of 2–4 cells (Fig. 6e and f). Very few DAPI-stained cells were observed at 2, 22 and 42 cmbsf. None of these cells showed a positive signal for any of the ANME probes. Below 50 cmbsf, almost no DAPI-stained cells could be observed, and no ANME-1 cells were detected in the Mercator MV Crater Centre at the investigated depths. In contrast, in the AOM zone (30 cmbsf) of the CAMV Crater Centre, the presence of ANME-2 cells (previously found in the study by Niemann *et al.* (2006a) was confirmed by FISH assays. There, ANME-2 cells occurred as shell-type aggregates, surrounded by other non-ANME cells (Fig. 6g and h).

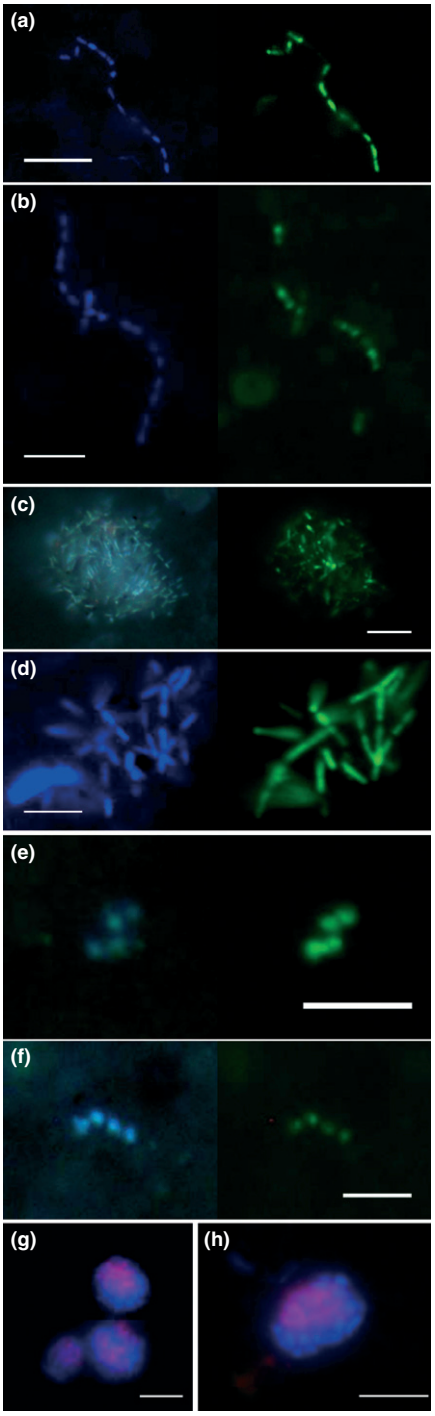

Fig. 6. Direct microscopic observations of AOM communities of CARD-FISH- and DAPI-stained cells at Mercator MV. Monospecific chains of rod-shaped cells positive for the ANME-1 probe (a and b), or aggregates comprising ANME-1 positive cells (c and d) observed at Mercator MV Crater Rim 1 (32 cmbsf). (e and f) small cocci or short rod-shaped ANME-1 positive cells observed at Mercator MV Crater Rim 2 (41 cmbsf). Overlay of DAPI-stained (blue) and ANME-2/Cy3 (red)-stained cells images (double-stained cells appear in purple). White scale bars: 5 μm.

Discussion

AOM activity in hypersaline and nonhypersaline sediments

AOM activity in extreme hypersaline environments

Hypersaline milieus are typically considered as hostile or even biogeochemical dead ends. Although the immense

ionic strength and osmotic pressure appear to exclude most life on Earth, some specialized microorganisms and a few Eukarya have adapted to minimize the negative effects of hypersalinity. This allowed them to thrive in these extremely challenging environments (Boetius & Joye, 2009). Because of the many biochemical constraints associated with life in hypersalinity, these environments are believed to select for metabolisms associated with elevated energy yield. In contrast, AOM is characterized by one of the lowest known energy yields among microbial energy conserving reactions. In the particular case of the putative syntrophic nature of AOM, the energy is shared, which further reduces the energy yield for each syntrophic partner. Despite these constraints, previous studies have shown that AOM can occur in hypersaline environments such as Mono- (Joye *et al.*, 1999) and Big Soda lake (Iversen *et al.*, 1987) at salinity of 88–90 g L^{-1} (*c.* 1.6 M Cl^-). In marine cold seep sediments, Lloyd *et al.* (2006) provided geochemical and molecular evidence for AOM activity at 146 g L^{-1} (*c.* 2.5 M Cl^-). Our results significantly extend the salinity range for AOM, showing that substantial rates (2.3 nmol cm^{-3} day^{-1} at Mercator MV Crater Centre) can be attained under extreme hypersaline conditions of 263 g L^{-1} (4.5 M Cl^-), and even at halite-saturating conditions (340 g L^{-1} or 5.8 M Cl^-) with rates of 0.5 nmol cm^{-3} day^{-1}. Hence, ANME-1 cells detected in extreme hypersaline environments, such as the Bannock, l'Atalante and Thetis deep-sea brine pools, with respective salinities of 148 g L^{-1} (Daffonchio *et al.*, 2006), 230 g L^{-1} (Yakimov *et al.*, 2007) and 348 g L^{-1} (La Cono *et al.*, 2011), might well perform AOM. However, these results are in contrast with the current concept that hypersaline conditions select for high-energy yield metabolisms. It is not clear how microbial communities mediating AOM can implement energy demanding osmoregulatory mechanisms (e.g. ion pumping or production of compatible solutes) unless the low AOM energy yield is balanced by a very high methane turnover per cell.

Evidence for a salt-induced AOM inhibition

At Mercator MV, maximum AOMR were below 8.5 nmol cm^3 day^{-1}, and even as low as 2.3 nmol cm^3 day^{-1} in the most hypersaline Crater Centre site. This later value is approximately five times lower than maximum AOMR in nonhypersaline sediments of CAMV (11.4 nmol cm^{-3} day^{-1}, this study), and even *c.* 150 times lower than maximum rates reported in a mud volcano (e.g. 350 nmol cm^{-3} day^{-1} under the *beggiatoa* mat at the Haakon Mosby MV in the Barent Sea; Niemann *et al.*, 2006b). These results were unexpected because AOM rates amplitude is generally controlled by methane and sulphate availability in sediments (Dale *et al.*, 2008; Knab *et al.*, 2009). However, sulphate and methane concentrations were much higher in Mercator MV than in the SMTZ of AOM zones at other cold seep sites (Knittel & Boetius, 2009 and references therein). The presence of such large sulphate and methane pools would thus have the potential to sustain much higher rates than the one observed in the hypersaline sites. This strongly suggests that AOM was inhibited at the level of cell activity or population growth, probably as a result of the extreme hypersaline conditions at Mercator MV. Further evidence for a salinity-induced inhibition of AOM is given by comparing Mercator MV sites. At Rim 1 and 2 sites where salinity was lower than in the Crater Centre, maximum AOMR were higher in spite of the lower methane concentration. These higher rates resulted in an almost complete consumption of methane below the sediment surface, unlike at the Crater Centre site where methane was not entirely consumed in the sediments. This interpretation of a salinity-induced inhibition of AOM activity is further supported by the results of Nauhaus *et al.* (2005) showing that AOM rates tend to decrease with increasing salt concentration above sea water salinity during *in vitro* incubations with seep sediments.

AOM inhibition and multiple sulphate sources lead to an unusual microbial activity spatial distribution

AOM activity at all Mercator MV sites displayed a much wider vertical distribution than in typical SMTZ where AOM activity is confined to a discrete sediment horizon (Knittel & Boetius, 2009), as observed in CAMV site with background salinity. Mercator MV hypersaline sediments were characterized by elevated sulphate levels because of the leaching of sulphate-rich evaporites by the ascending fluid (Scholz *et al.*, 2009). In this system, sulphate was therefore transported not only downward from sea water into the sediment, but also upward together with other ions, hydrocarbons and geofluids. The multiple sources of sulphate in this original system, combined with the hypersalinity-induced inhibition of AOM that prevents depletion of both sulphate and methane (see above), can thus explain the unusually broad microbial activity distribution. Interestingly, despite higher maximum AOMR at CAMV, depth integrated areal rates ($\sum$AOMR) were 6.1- and 3.8-fold lower than in Mercator MV Crater Centre and Rim 2, respectively (Table 2). Hence, such vertical extension of AOM activity resulted in higher turnover per unit area and thus compensated to some extent the reduction of volumetric rates.

Interpretation of Mercator MV biogeochemical structure and functioning

Decomposition of shallow subsurface methane hydrate is a widespread cause of high methane advective flux and gas

seepage from cold seep systems such as Hydrate Ridge (off Oregon) or Eel River Basin (off California). At Mercator MV, the observation of shallow subseafloor internal seismic reflectors resembling bottom-simulating reflectors suggested the presence of gas hydrates near the surface (Depreiter *et al.*, 2005). On the basis of these results and on video observations of gas venting from Mercator MV crater (Van Rooij *et al.*, 2005), it has been proposed that methane hydrate dissociation could also occur at this site (Van Rooij *et al.*, 2005). The present study thus provides new insights on the origin of the gas venting from Mercator MV Crater Centre. Our results indeed show that hypersaline conditions, by disrupting the so-called 'methane benthic filter', was the main cause of methane venting in the water column.

AOM community structure in hypersaline sediments of Mercator MV

ANME-1 as a hypersaline anaerobic methanotroph ecotype

The Mercator MV environment closely resembles the Gulf of Mexico gassy sediment described in the study by Lloyd *et al.* (2006), in term of hypersalinity and dominance of ANME-1 cells. Therefore, extremely saline environments may well exert a selective pressure towards ANME-1, as already proposed in the study by Lloyd *et al.* (2006) and Yakimov *et al.* (2007). This would also explain the findings of ANME-1 in brines in the Eastern Mediterranean (Daffonchio *et al.*, 2006; Yakimov *et al.*, 2007; La Cono *et al.*, 2011). As ANME-1 cells have also been reported at the CAMV Crater Centre site (Niemann *et al.*, 2006a) and other nonhypersaline environments (see Data S1 and Knittel & Boetius, 2009), a negative selection towards other ANME groups thus appears to be the most probable ANME selection mechanism in hypersaline cold seeps.

Such selection pattern could be related to the comparatively low effect of ionic strength on Archaea in general and ANME-1 in particular. The permeability of archaeal membranes comprising isoprenoidal glycerol ethers is generally lower than that of bacterial membranes comprising fatty acid glycerol esters (Valentine, 2007). Low membrane permeability reduces the energy loss associated with random ion exchange between the cyto- and ectoplasm. Specifically, ANME-1 comprises high contents of membrane-spanning lipids, so-called glycerol dialkyl glycerol tetraethers-GDGTs (Niemann & Elvert, 2008 and references therein). Membranes composed of GDGTs are at the lower end of permeability when comparing typical membrane lipids (Yamauchi *et al.*, 1993; Valentine, 2007). In contrast, ANME-2 and -3 cell membranes rather contain diethers, that are characterized by higher permeability, and less or no GDGTs (Rossel *et al.*, 2011). This could thus explain why hypersalinity seems to exclude ANME-2 and ANME-3 but not ANME-1 cells. In addition, genes coding for mannosylglycerate and di-myo-inositol-phosphate synthesis pathways were identified in the ANME-1 genome (Meyerdierks *et al.*, 2010). These two compatible solutes are widely employed by halophilic microorganisms to increase their turgor pressure (Roberts, 2004; da Costa & Empadinhas, 2008). These compounds may thus also confer hypersalinity adaptation to the ANME-1 cells. Finally, Stokke *et al.* (2012) recently unravelled the presence of proteins from ANME-1 involved in rigid gas vesicle synthesis that could constitute a salt stress response.

On the syntrophic nature of AOM in Mercator MV sediments

In Mercator MV Rim 1 sediments, ANME-1 cells were mainly present as monospecific chains, with no apparent contact with any other cell type. In addition, the ANME/DSS ratio was of 7 : 1 (29 cmbsf in Mercator MV Rim 1), strongly differing from the typical 1 : 1 to 1 : 3 ratios observed in shell-type consortia (Boetius *et al.*, 2000; Orcutt & Meile, 2008). As no other putative anaerobic methanotrophs were detected in Mercator MV sediments, our results suggest that ANME-1 cells at Mercator MV can mediate AOM, even in the absence of ANME-2- or ANME-3-like consortia with SRB (see Data S1 for a short review of ANME-1 organization at other seep sites). However, despite our observations of a few large ANME-1 clusters (Fig. 6c and d), the disaggregation of cell assemblage by CARD-FISH preparation cannot be ruled out. At Mercator Crater Centre site, the absence of ANME cells indicates that methane oxidation observed in the first 50 cm was probably not carried out by any known ANME cell type. Below 50 cmbsf, sediments were more hypersaline, and it is possible that cell fixation involving sea water salinity reagents (see Materials and methods) caused osmotic shocks and substantial cell lysis in these samples. This could explain that DAPI-stained cells were rarely observed in these samples despite significant activity rates.

Reaction coupling between AOM, SR and MG

Sulphate-dependant AOM

At CAMV Crater Centre, we found that depth of SRR and AOMR maxima coincided, and areal SRR ($\sum$SRR) exceeded areal AOMR ($\sum$AOMR) within the SMTZ. On the basis of these areal rates, 63% of the SR in the AOM zone was because of methane oxidation (Table 2). This was thus compatible with a coupling between these reactions with an equimolar consumption of both substrates.

Several factors can account for the remaining 37% SR activity in the AOM zone: organoclastic SR through mineralization of higher hydrocarbons comigrating with methane (Niemann *et al.*, 2006a; Kniemeyer *et al.*, 2007; Bowles *et al.*, 2011) or sedimentary organic matter from microbial or seep fauna necromass (Niemann *et al.*, 2006a; Hilario & Cunha, 2008; Sommer *et al.*, 2009).

Evidence of alternative electron acceptors for AOM

We also found the reverse situation where ∑AOMR consistently exceeded ∑SRR over large depth intervals at Mercator MV Crater Centre or Rim 2 and at CAMV Crater Centre between 43 and 300 cmbsf. These remarkable results suggested the presence of alternative electron acceptors, other than sulphate, in both MV sediments. No nitrate/nitrite was detected in any anion-exchange chromatograms (results not shown), suggesting that N-dependant AOM (Raghoebarsing *et al.*, 2006; Beal *et al.*, 2009; Ettwig *et al.*, 2010) is unlikely involved in methane turnover at this site. The presence of a large pool of Fe is suggested by the presence of significant AVS concentration, at least in Rim1 station. Fe(III) can be present in subseafloor sediments and brines (D'Hondt *et al.*, 2004; Parkes *et al.*, 2005) and has been shown to be responsible of a cryptic sulphur cycle through sulphide reoxidation (Holmkvist, *et al.*, 2011). Although speculative at present, it therefore seems possible that AOM at Mercator MV partially rely on other electron acceptors than sulphate. At CAMV, the intrusion of sea water within the ascending fluid (Hensen *et al.*, 2007) could be the source of such electron acceptors.

Interestingly, similar decoupling of AOM and SR was already observed in conditions of very low or no sulphate, either *in vitro* (Hansen *et al.*, 1998; Beal *et al.*, 2011) or in environmental samples, at the base of or below SMTZs (Hansen *et al.*, 1998; Joye *et al.*, 2004; Niemann *et al.*, 2006a; Parkes *et al.*, 2007), which apparently correspond to the preferential habitat for ANME-1 cells in nonhypersaline methane–bearing marine sediments (Knittel *et al.*, 2005; Yanagawa *et al.*, 2011). These observations suggest that ANME-1-dominated AOM communities could potentially decouple AOM and SR, as observed in the present study.

Methanogenesis rates and zonation

Populations of ANME cells can have a dual methanotrophic–methanogenic activity, as evidenced by environmental surveys (Orcutt *et al.*, 2005) or *in vitro* incubations (Treude *et al.*, 2007; Orcutt & Meile, 2008). In both MV of this study, zones of methanogenic activity did not overlap with methanotrophic activity. Hence, MG rates measured here are rather attributed to 'true' MG instead of methanotrophic 'coreaction'. In any cases, MG activity was too low and within too narrow sediment intervals to significantly contribute to the methane pool at all investigated sites.

In the presence of sulphate, SRB generally outcompete methanogens for the utilization of H_2 or acetate (Kristjansson *et al.*, 1982; Schonheit *et al.*, 1982). In line with this general rule was the presence of Ac-MG rates only below the SMTZ at CAMV Crater Centre, where sulphate was depleted. However, peaks of Ac-MG and H-MG also occurred in the sulphate zone in Mercator MV Rim 1 sediments, thus departing from such typical zonation. Similar results were reported in the Napoli MV hypersaline sediments of the East Mediterranean sea (Lazar *et al.*, 2011). In the presence of sulphate, methylotrophic methanogens can still metabolize methyl moieties but mostly redirect them through the reverse MG oxidative pathway, with CO_2 as final product rather than CH_4 (Finke *et al.*, 2007). In this case, SR acts as a sink for the electrons released during methyl oxidation via interspecies H_2 transfer. Similar process could occur with acetate as electron donor (Phelps *et al.*, 1985; Achtnich *et al.*, 1995) and could explain the residual Ac-MG rate observed at Mercator MV Rim 1. This interpretation of residual Ac-MG was supported by an important peak of acetate oxidation to CO_2 at 13 cmbsf (7847 pmol cm^{-3} day^{-1}, data not shown) compared to the CH_4 formation (2.4 pmol cm^{-3} day^{-1}) at the same depth. The interpretation of the H-MG activity peak was more problematic, as SRB usually maintain H_2 levels that are inhibitory for methanogens (Kristjansson *et al.*, 1982). The Met-MG activity in sulphate-rich near-surface sediments at all sites excepted Mercator MV Crater Centre was coherent with the fact that methylated amines are noncompetitive substrate that cannot be used by SRB (Oremland & Polcin, 1982).

Conclusion

In brine sediments of Mercator MV, the abundance of both sulphate and methane in the ascending fluid fuels substantial rates of AOM and SR. Unlike in typical methane-bearing sediments, no clear SMTZ is present, and AOM and SR are distributed over wide depth intervals. However, hypersaline conditions partially inhibited AOM such that maximum volumetric rates are orders of magnitude lower in comparison with other cold seeps. At Mercator MV, AOM is mediated by ANME-1, which mostly occurs as monospecific cell chains and constitutes up to four-fifth of the microbial community. This, together with previous findings of ANME-1 in hypersaline settings, suggests that this ANME clade is well adapted to elevated salinity despite the low energy conserved from the AOM reaction. We also found that AOM and SR can be uncou-

pled with AOM significantly exceeding SR over wide depth intervals. Hypothetically, this could be related to the utilization of electron acceptors other than sulphate for AOM.

Acknowledgements

This work was supported by the 'HERMES' project grant (Hot-Spot Ecosystems along European Margins) under FP6 of the European Commission, the European Science Foundation 'MicroSystems' grant (FWO-506G.0656.05) and the Geconcerteerde Onderzoeksactie (GOA) of Ghent University (BOF09/GOA/005). L.M. was recipient of a PhD grant from the 'Institute for the Promotion of Innovation by Science and Technology in Flanders' (IWT-Vlaanderen, contract number SB-53575). We wish to acknowledge the contribution of the crew and scientific party of the MSM1/3 cruise led by O. Pfannkuche aboard the RV Maria S. Merian (2006), who largely contributed to the preliminary results enabling this work. The authors would like to thank the shipboard scientific party and crew of the Research Vessel 'James Cook' (JC10 cruise) and the ROV ISIS pilots/engineers. They contributed to this study with their valuable on-board assistance and long seafloor video observations shifts. In particular, K. Heeschen and V. Hühnerbach are thanked for cruise organization and for on-board data handling, respectively. We thank W. Verstraete for helpful suggestions and M. Mußmann for assistance with CARD-FISH assays. The authors declare that they have no conflict of interest.

References

Achtnich C, Schuhmann A, Wind T & Conrad R (1995) Role of interspecies H-2 transfer to sulfate and ferric iron-reducing bacteria in acetate consumption in anoxic paddy soil. *FEMS Microbiol Ecol* **16**: 61–69.

Anisimova M & Gascuel O (2006) Approximate likelihood-ratio test for branches: a fast, accurate, and powerful alternative. *Syst Biol* **55**: 539–552.

Beal EJ, House CH & Orphan VJ (2009) Manganese- and iron-dependent marine methane oxidation. *Science* **325**: 184–187.

Beal EJ, Claire MW & House CH (2011) High rates of anaerobic methanotrophy at low sulfate concentrations with implications for past and present methane levels. *Geobiology* **9**: 131–139.

Boetius A & Joye S (2009) Thriving in salt. *Science* **324**: 1523–1525.

Boetius A, Ravenschlag K, Schubert CJ *et al.* (2000) A marine microbial consortium apparently mediating anaerobic oxidation of methane. *Nature* **407**: 623–626.

Bowles MW, Samarkin VA, Bowles KM & Joye SB (2011) Weak coupling between sulfate reduction and the anaerobic oxidation of methane in methane-rich seafloor sediments during *ex situ* incubation. *Geochim Cosmochim Acta* **75**: 500–519.

Cline JD (1969) Spectrophotometric determination of hydrogen sulfide in natural waters. *Limnol Oceanogr* **14**: 454–458.

da Costa MS & Empadinhas N (2008) Osmoadaptation mechanisms in prokaryotes: distribution of compatible solutes. *Int Microbiol* **11**: 151–161.

Daffonchio D, Borin S, Brusa T *et al.* (2006) Stratified prokaryote network in the oxic-anoxic transition of a deep-sea halocline. *Nature* **440**: 203–207.

Daims H, Bruhl A, Amann R, Schleifer KH & Wagner M (1999) The domain-specific probe EUB338 is insufficient for the detection of all Bacteria: development and evaluation of a more comprehensive probe set. *Syst Appl Microbiol* **22**: 434–444.

Dale AW, Regnier P, Knab NJ, Jørgensen BB & Van Cappellen P (2008) Anaerobic oxidation of methane (AOM) in marine sediments from the Skagerrak (Denmark): II. Reaction-transport modeling. *Geochim Cosmochim Acta* **72**: 2880–2894.

Depreiter D, Poort J, Van Rensbergen P & Henriet JP (2005) Geophysical evidence of gas hydrates in shallow submarine mud volcanoes on the Moroccan margin. *J Geophys Res* **110**: B10103.

D'Hondt S, Jorgensen BB, Miller DJ *et al.* (2004) Distributions of microbial activities in deep subseafloor sediments. *Science* **306**: 2216–2221.

Dimitrov LI (2002) Mud volcanoes – the most important pathway for degassing deeply buried sediments. *Earth Sci Rev* **59**: 49–76.

Duan ZH & Mao SD (2006) A thermodynamic model for calculating methane solubility, density and gas phase composition of methane-bearing aqueous fluids from 273 to 523 K and from 1 to 2000 bar. *Geochim Cosmochim Acta* **70**: 3369–3386.

Ettwig KF, Butler MK, Le Paslier D, *et al.* (2010) Nitrite-driven anaerobic methane oxidation by oxygenic bacteria. *Nature* **464**: 543–548.

Finke N, Hoehler TM & Jorgensen BB (2007) Hydrogen 'leakage' during methanogenesis from methanol and methylamine: implications for anaerobic carbon degradation pathways in aquatic sediments. *Environ Microbiol* **9**: 1060–1071.

Guindon S, Dufayard JF, Hordijk W, Lefort V & Gascuel O (2009) PhyML: fast and accurate phylogeny reconstruction by maximum likelihood. *Infect Genet Evol* **9**: 384–385.

Hall PO & Aller RC (1992) Rapid, small-volume, flow-injection analysis for sigma-CO2 and NH4+ in marine and fresh-waters. *Limnol Oceanogr* **37**: 1113–1119.

Hansen LB, Finster K, Fossing H & Iversen N (1998) Anaerobic methane oxidation in sulfate depleted sediments: effects of sulfate and molybdate additions. *Aquat Microb Ecol* **14**: 195–204.

Hensen C, Nuzzo M, Hornibrook E, Pinheiro LM, Bock B, Magalhaes VH & Bruckmann W (2007) Sources of mud volcano fluids in the Gulf of Cadiz - indications for hydrothermal imprint. *Geochim Cosmochim Acta* **71**: 1232–1248.

Hilario A & Cunha MR (2008) On some frenulate species (Annelida : Polychaeta : Siboglinidae) from mud volcanoes in the Gulf of Cadiz (NE Atlantic). *Sci Mar* **72**: 361–371.

Hinrichs KU, Hayes JM, Sylva SP, Brewer PG & DeLong EF (1999) Methane-consuming archaebacteria in marine sediments. *Nature* **398**: 802–805.

Holmkvist L, Ferdelman TG & Jorgensen BB (2011) A cryptic sulfur cycle driven by iron in the methane zone of marine sediment (Aarhus Bay, Denmark). *Geochimica et Cosmochimica Acta* **75**: 3581–3599.

Hu SH, Zeng RJ, Burow LC, Lant P, Keller J & Yuan ZG (2009) Enrichment of denitrifying anaerobic methane oxidizing microorganisms. *Environ Microbiol Rep* **1**: 377–384.

Iversen N, Oremland RS & Klug MJ (1987) Big Soda Lake (Nevada). 3. Pelagic methanogenesis and anaerobic methane oxidation. *Limnol Oceanogr* **32**: 804–814.

Jørgensen BB (1978) Comparison of methods for the quantification of bacterial sulfate reduction in coastal marine-sediments. 1. Measurement with radiotracer techniques. *Geomicrobiol J* **1**: 11–27.

Joye SB, Connell TL, Miller LG, Oremland RS & Jellison RS (1999) Oxidation of ammonia and methane in an alkaline, saline lake. *Limnol Oceanogr* **44**: 178–188.

Joye SB, Boetius A, Orcutt BN, Montoya JP, Schulz HN, Erickson MJ & Lugo SK (2004) The anaerobic oxidation of methane and sulfate reduction in sediments from Gulf of Mexico cold seeps. *Chem Geol* **205**: 219–238.

Joye SB, Samarkin VA, Orcutt BN *et al.* (2009) Metabolic variability in seafloor brines revealed by carbon and sulphur dynamics. *Nat Geosci* **2**: 349–354.

Kallmeyer J, Ferdelman TG, Weber A, Fossing H & Jorgensen BB (2004) A cold chromium distillation procedure for radiolabeled sulfide applied to sulfate reduction measurements. *Limnol Oceanogr Methods* **2**: 171–180.

Kane MD, Poulsen LK & Stahl DA (1993) Monitoring the enrichment and isolation of sulfate-reducing bacteria by using oligonucleotide hybridization probes designed from environmentally derived 16S ribosomal-RNA sequences. *Appl Environ Microbiol* **59**: 682–686.

Knab NJ, Cragg BA, Hornibrook ERC *et al.* (2009) Regulation of anaerobic methane oxidation in sediments of the Black Sea. *Biogeosciences* **6**: 1505–1518.

Kniemeyer O, Musat F, Sievert SM *et al.* (2007) Anaerobic oxidation of short-chain hydrocarbons by marine sulphate-reducing bacteria. *Nature* **449**: 898–910.

Knittel K & Boetius A (2009) Anaerobic oxidation of methane: progress with an unknown process. *Annu Rev Microbiol* **63**: 311–334.

Knittel K, Boetius A, Lemke A *et al.* (2003) Activity, distribution, and diversity of sulfate reducers and other bacteria in sediments above gas hydrate (Cascadia margin, Oregon). *Geomicrobiol J* **20**: 269–294.

Knittel K, Losekann T, Boetius A, Kort R & Amann R (2005) Diversity and distribution of methanotrophic archaea at cold seeps. *Appl Environ Microbiol* **71**: 467–479.

Kopf AJ (2002) Significance of mud volcanism. *Rev Geophys* **B40**: 1–49.

Kristjansson JK, Schonheit P & Thauer RK (1982) Different Ks-values for hydrogen of methanogenic bacteria and sulfate reducing bacteria - an explanation for the apparent inhibition of methanogenesis by sulfate. *Arch Microbiol* **131**: 278–282.

La Cono V, Smedile F, Bortoluzzi G *et al.* (2011) Unveiling microbial life in new deep-sea hypersaline Lake Thetis. Part I: prokaryotes and environmental settings. *Environ Microbiol* **13**: 2250–2268.

Lazar CS, Parkes RJ, Cragg BA, L'Haridon S & Toffin L (2011) Methanogenic diversity and activity in hypersaline sediments of the centre of the Napoli mud volcano, Eastern Mediterranean Sea. *Environ Microbiol* **13**: 2078–2091.

Lloyd KG, Lapham L & Teske A (2006) Anaerobic methane-oxidizing community of ANME-1b archaea in hypersaline Gulf of Mexico sediments. *Appl Environ Microbiol* **72**: 7218–7230.

Losekann T, Knittel K, Nadalig T, Fuchs B, Niemann H, Boetius A & Amann R (2007) Diversity and abundance of aerobic and anaerobic methane oxidizers at the Haakon Mosby mud volcano, Barents Sea. *Appl Environ Microbiol* **73**: 3348–3362.

Manz W, Eisenbrecher M, Neu TR & Szewzyk U (1998) Abundance and spatial organization of Gram-negative sulfate-reducing bacteria in activated sludge investigated by *in situ* probing with specific 16S rRNA targeted oligonucleotides. *FEMS Microbiol Ecol* **25**: 43–61.

Massana R, Murray AE, Preston CM & DeLong EF (1997) Vertical distribution and phylogenetic characterization of marine planktonic Archaea in the Santa Barbara Channel. *Appl Environ Microbiol* **63**: 50–56.

Meyerdierks A, Kube M, Kostadinov I, Teeling H, Glockner FO, Reinhardt R & Amann R (2010) Metagenome and mRNA expression analyses of anaerobic methanotrophic archaea of the ANME-1 group. *Environ Microbiol* **12**: 422–439.

Milkov AV (2000) Worldwide distribution of submarine mud volcanoes and associated gas hydrates. *Mar Geol* **167**: 29–42.

Mills HJ, Hodges C, Wilson K, MacDonald IR & Sobecky PA (2003) Microbial diversity in sediments associated with surface-breaching gas hydrate mounds in the Gulf of Mexico. *FEMS Microbiol Ecol* **46**: 39–52.

Mills HJ, Martinez RJ, Story S & Sobecky PA (2004) Identification of members of the metabolically active microbial populations associated with Beggiatoa species mat communities form Gulf of Mexico cold-seep sediments. *Appl Environ Microbiol* **70**: 5447–5458.

Muyzer G, Teske A, Wirsen CO & Jannasch HW (1995) Phylogenetic-relationships of thiomicrospira species and their identification in deep-sea hydrothermal vent samples by denaturing gradient gel-electrophoresis of 16S rDNA fragments. *Arch Microbiol* **164**: 165–172.

Nauhaus K, Treude T, Boetius A & Kruger M (2005) Environmental regulation of the anaerobic oxidation of

methane: a comparison of ANME-I and ANME-II communities. *Environ Microbiol* **7**: 98–106.

Niederberger TD, Perreault NN, Tille S *et al.* (2010) Microbial characterization of a subzero, hypersaline methane seep in the Canadian High Arctic. *ISME J* **4**: 1326–1339.

Niemann H & Boetius A (2010) Mud volcanoes. *Handbook of Hydrocarbon and Lipid Microbiology* (Timmis KN, ed), pp. 205–214. Springer, Berlin, Heidelberg.

Niemann H & Elvert M (2008) Diagnostic lipid biomarker and stable carbon isotope signatures of microbial communities mediating the anaerobic oxidation of methane with sulphate. *Org Geochem* **39**: 1668–1677.

Niemann H, Elvert M, Hovland M *et al.* (2005) Methane emission and consumption at a North Sea gas seep (Tommeliten area). *Biogeosciences* **2**: 335–351.

Niemann H, Duarte J, Hensen C *et al.* (2006a) Microbial methane turnover at mud volcanoes of the Gulf of Cadiz. *Geochim Cosmochim Acta* **70**: 5336–5355.

Niemann H, Losekann T, de Beer D *et al.* (2006b) Novel microbial communities of the Haakon Mosby mud volcano and their role as a methane sink. *Nature* **443**: 854–858.

Nuzzo M, Hornibrook ERC, Gill F *et al.* (2009) Origin of light volatile hydrocarbon gases in mud volcano fluids, Gulf of Cadiz – evidence for multiple sources and transport mechanisms in active sedimentary wedges. *Chem Geol* **266**: 359–372.

Orcutt B & Meile C (2008) Constraints on mechanisms and rates of anaerobic oxidation of methane by microbial consortia: process-based modeling of ANME-2 archaea and sulfate reducing bacteria interactions. *Biogeosciences* **5**: 1587–1599.

Orcutt B, Boetius A, Elvert M, Samarkin V & Joye SB (2005) Molecular biogeochemistry of sulfate reduction, methanogenesis and the anaerobic oxidation of methane at Gulf of Mexico cold seeps. *Geochim Cosmochim Acta* **69**: 4267–4281.

Oremland RS & Polcin S (1982) Methanogenesis and sulfate reduction – competitive and noncompetitive substrates in estuarine sediments. *Appl Environ Microbiol* **44**: 1270–1276.

Oren A (1999) Bioenergetic aspects of halophilism. *Microbiol Mol Biol Rev* **63**: 334–348.

Oren A (2011) Thermodynamic limits to microbial life at high salt concentrations. *Environ Microbiol* **13**: 1908–1923.

Orphan VJ, House CH, Hinrichs KU, McKeegan KD & DeLong EF (2001) Methane-consuming archaea revealed by directly coupled isotopic and phylogenetic analysis. *Science* **293**: 484–487.

Orphan VJ, House CH, Hinrichs KU, McKeegan KD & DeLong EF (2002) Multiple archaeal groups mediate methane oxidation in anoxic cold seep sediments. *Proc Nat Acad Sci USA* **99**: 7663–7668.

Parkes RJ, Webster G, Cragg BA *et al.* (2005) Deep sub-seafloor prokaryotes stimulated at interfaces over geological time. *Nature* **436**: 390–394.

Parkes RJ, Cragg BA, Banning N *et al.* (2007) Biogeochemistry and biodiversity of methane cycling in subsurface marine sediments (Skagerrak, Denmark). *Environ Microbiol* **9**: 1146–1161.

Perez-Garcia C, Berndt C, Klaeschen D, Mienert J, Haffert L, Depreiter D & Haeckel M (2011) Linked halokinesis and mud volcanism at the Mercator mud volcano, Gulf of Cadiz. *J Geophys Res* **116**: B05101.

Pernthaler J, Glockner FO, Schonhuber W & Amann R (2001) Fluorescence *in situ* hybridization (FISH) with rRNA-targeted oligonucleotide probes. *Methods Microbiol* **30**: 207–226.

Pernthaler A, Pernthaler J & Amann R (2002) Fluorescence *in situ* hybridization and catalyzed reporter deposition for the identification of marine bacteria. *Appl Environ Microbiol* **68**: 3094–3101.

Phelps TJ, Conrad R & Zeikus JG (1985) Sulfate-dependent interspecies H-2 transfer between Methanosarcina-Barkeri and Desulfovibrio-Vulgaris during coculture metabolism of acetate or methanol. *Appl Environ Microbiol* **50**: 589–594.

Pruesse E, Quast C, Knittel K, Fuchs BM, Ludwig WG, Peplies J & Glockner FO (2007) SILVA: a comprehensive online resource for quality checked and aligned ribosomal RNA sequence data compatible with ARB. *Nucleic Acids Res* **35**: 7188–7196.

Raghoebarsing AA, Pol A, van de Pas-Schoonen KT *et al.* (2006) A microbial consortium couples anaerobic methane oxidation to denitrification. *Nature* **440**: 918–921.

Reeburgh WS (1967) An improved interstitial water sampler. *Limnol Oceanogr* **12**: 163–165.

Reeburgh WS (2007) Oceanic methane biogeochemistry. *Chem Rev* **107**: 486–513.

Roberts MF (2004) Osmoadaptation and osmoregulation in archaea: update 2004. *Front Biosci* **9**: 1999–2019.

Rossel PE, Elvert M, Ramette A, Boetius A & Hinrichs KU (2011) Factors controlling the distribution of anaerobic methanotrophic communities in marine environments: evidence from intact polar membrane lipids. *Geochim Cosmochim Acta* **75**: 164–184.

Schloss PD, Westcott SL, Ryabin T *et al.* (2009) Introducing mothur: open-source, platform-independent, community-supported software for describing and comparing microbial communities. *Appl Environ Microbiol* **75**: 7537–7541.

Scholz F, Hensen C, Reitz A *et al.* (2009) Isotopic evidence (Sr-87/Sr-86, delta Li-7) for alteration of the oceanic crust at deep-rooted mud volcanoes in the Gulf of Cadiz, NE Atlantic Ocean. *Geochim Cosmochim Acta* **73**: 5444–5459.

Schonheit P, Kristjansson JK & Thauer RK (1982) Kinetic mechanism for the ability of sulfate reducers to out-compete methanogens for acetate. *Arch Microbiol* **132**: 285–288.

Schreiber L, Holler T, Knittel K, Meyerdierks A & Amann R (2010) Identification of the dominant sulfate-reducing bacterial partner of anaerobic methanotrophs of the ANME-2 clade. *Environ Microbiol* **12**: 2327–2340.

Sommer S, Linke P, Pfannkuche O *et al.* (2009) Seabed methane emissions and the habitat of frenulate tubeworms on the Captain Arutyunov mud volcano (Gulf of Cadiz). *Mar Ecol Prog Ser* **382**: 69–86.

Stahl DA & Amann RI (1991) Development and application of nucleic acid probes in bacterial systematics. *Nucleic Acid Techniques in Bacterial Systematics* (Stackebrandt E & Goodfellow M, eds), pp. 205–248. John Wiley & Sons Ltd, Chichester, UK.

Stokke R, Roalkvam I, Lanzen A, Haflidason H & Steen IH (2012) Integrated metagenomic and metaproteomic analyses of an ANME-1-dominated community in marine cold seep sediments. *Environ Microbiol* **14**: 1333–1346.

Treude T, Boetius A, Knittel K, Wallmann K & Jorgensen BB (2003) Anaerobic oxidation of methane above gas hydrates at Hydrate Ridge, NE Pacific Ocean. *Mar Ecol Prog Ser* **264**: 1–14.

Treude T, Knittel K, Blumenberg M, Seifert R & Boetius A (2005) Subsurface microbial methanotrophic mats in the Black Sea. *Appl Environ Microbiol* **71**: 6375–6378.

Treude T, Orphan V, Knittel K, Gieseke A, House CH & Boetius A (2007) Consumption of methane and CO2 by methanotrophic microbial mats from gas seeps of the anoxic Black Sea. *Appl Environ Microbiol* **73**: 2271–2283.

Valentine DL (2007) Adaptations to energy stress dictate the ecology and evolution of the Archaea. *Nat Rev Microbiol* **5**: 316–323.

Van Rensbergen P, Depreiter D, Pannemans B *et al.* (2005) The El arraiche mud volcano field at the Moroccan Atlantic slope, Gulf of Cadiz. *Mar Geol* **219**: 1–17.

Van Rooij D, Depreiter D, Henriet JP *et al.* (2005) First sighting of active fluid venting in the Gulf of Cadiz. *EOS Trans AGU* **86**: 509.

Yakimov MM, La Cono V, Denaro R *et al.* (2007) Primary producing prokaryotic communities of brine, interface and seawater above the halocline of deep anoxic lake L'Atalante, Eastern Mediterranean Sea. *ISME J* **1**: 743–755.

Yamauchi K, Doi K, Yoshida Y & Kinoshita M (1993) Archaebacterial lipids – highly proton-impermeable membranes from 1,2-diphytanyl-sn-glycero-3-phosphocholine. *Biochim Biophys Acta* **1146**: 178–182.

Yanagawa K, Sunamura M, Lever MA *et al.* (2011) Niche separation of methanotrophic archaea (ANME-1 and-2) in methane-seep sediments of the Eastern Japan Sea Offshore Joetsu. *Geomicrobiol J* **28**: 118–129.

Supporting Information

Additional Supporting Information may be found in the online version of this article:

Data S1. Microbathymetry. Sampling site, seafloor observations and sedimentology. Libraries rarefaction curves. Review of abundance, distribution, and consortia structure involving ANME-1.

Please note: Wiley-Blackwell is not responsible for the content or functionality of any supporting materials supplied by the authors. Any queries (other than missing material) should be directed to the corresponding author for the article.